

Teleoperator-Aware and Safety-Critical Adaptive Nonlinear MPC for Shared Autonomy in Obstacle Avoidance of Legged Robots

Ruturaj Sambhus¹, Muneeb Ahmad¹, Basit Muhammad Imran¹, Sujith Vijayan²,
Dylan P. Losey¹, and Kaveh Akbari Hamed¹

Abstract—Ensuring safe and effective collaboration between humans and autonomous legged robots is a fundamental challenge in shared autonomy, particularly for teleoperated systems navigating cluttered environments. Conventional shared-control approaches often rely on fixed blending strategies that fail to capture the dynamics of legged locomotion and may compromise safety. This paper presents a teleoperator-aware, safety-critical, adaptive nonlinear model predictive control (ANMPC) framework for shared autonomy of quadrupedal robots in obstacle-avoidance tasks. The framework employs a fixed arbitration weight between human and robot actions but enhances this scheme by modeling the human input with a noisily rational Boltzmann model, whose parameters are adapted online using a projected gradient descent (PGD) law from observed joystick commands. Safety is enforced through control barrier function (CBF) constraints integrated into a computationally efficient NMPC, ensuring forward invariance of safe sets despite uncertainty in human behavior. The control architecture is hierarchical: a high-level CBF-based ANMPC (10 Hz) generates blended human–robot velocity references, a mid-level dynamics-aware NMPC (60 Hz) enforces reduced-order single rigid body (SRB) dynamics to track these references, and a low-level nonlinear whole-body controller (500 Hz) imposes the full-order dynamics via quadratic programming to track the mid-level trajectories. Extensive numerical and hardware experiments, together with a user study, on a Unitree Go2 quadrupedal robot validate the framework, demonstrating real-time obstacle avoidance, online learning of human intent parameters, and safe teleoperator collaboration.

I. INTRODUCTION

Legged robots are increasingly envisioned as collaborative agents in disaster response, search-and-rescue, and other safety-critical domains where fully autonomous operation remains challenging. In such environments, *shared autonomy*—the integration of human teleoperation with autonomous decision-making—offers a promising paradigm that combines human intuition with robotic precision. Nevertheless, achieving effective shared autonomy for legged robots is nontrivial: human inputs are often noisy and unpredictable, while autonomous algorithms must simultaneously ensure safety in cluttered, dynamic environments. Compounding these challenges, legged robots themselves are inherently unstable systems, characterized by high degrees

The work of R. Sambhus, M. Ahmad, S. Vijayan, and K. Akbari Hamed is partially supported by the NSF under Grant 2423725.

¹R. Sambhus, M. Ahmad, B. Imran, D. Losey, and K. Akbari Hamed (*Corresponding Author*) are with the Department of Mechanical Engineering, Virginia Tech, Blacksburg, VA 24061, USA, {rutarajsambhus, muneeb24, basit, losey, kavehakbarihamed}@vt.edu

²S. Vijayan is with the School of Neuroscience, Virginia Tech, Blacksburg, VA 24061, USA, neuron99@vt.edu

of freedom (DoF), underactuation, unilateral contact constraints, and hybrid dynamics arising from contact switching.

A. Related Work

To address these challenges, model predictive control (MPC) techniques have emerged as a powerful tool for trajectory optimization and control of legged robots. In particular, MPC has been effectively integrated with reduced-order, or template, models [1], which provide low-dimensional abstractions of the complex, nonlinear dynamics of legged locomotion. Prominent examples include the linear inverted pendulum (LIP) model [2] and its extensions, such as the angular momentum LIP [3], spring-loaded inverted pendulum (SLIP) [4], vertical LIP [5], and hybrid LIP [6]. Other widely used formulations include centroidal dynamics [7] and the single rigid body (SRB) model [8]–[12]. While quadratic programming (QP)-based MPC formulations for linearized template models are computationally efficient, they struggle to incorporate nonlinear effects and enforce collision avoidance. This limitation has motivated the development of nonlinear MPC (NMPC) frameworks [13], [14], which directly account for nonlinear robot dynamics and safety constraints. NMPC has been successfully applied to gait planning and safety-critical locomotion of legged robots, see, e.g., [15]–[20].

Control barrier functions (CBFs) provide formal guarantees of safety for robotic systems [21]. In their standard form, CBFs are implemented as zero-horizon, QP-based controllers that minimally modify a nominal control law while enforcing safety constraints [22]. More recently, CBFs have been integrated with MPC to extend these guarantees over a nonzero prediction horizon, enabling safe motion planning for quadrupedal robots [14], [16], [17] and even car racing systems [23]. Despite these advances, most existing MPC/NMPC frameworks for legged robots assume fully autonomous operation and do *not* explicitly incorporate human-in-the-loop shared autonomy or intent modeling.

Shared autonomy has been widely studied in the context of teleoperation, where the goal is to combine human intuition with robotic autonomy. In general, shared autonomy focuses on balancing the human’s high-level knowledge (e.g., the goal the system should reach) with the robot’s low-level automation (e.g., the motions to reach that goal) [25]–[27]. A variety of shared autonomy algorithms have been developed for robot arms [28], [29], quadrotors [30], and smart vehicles [31]. However, these methods are not directly applicable to legged robots, where safe and effective operation requires



Fig. 1. Side-view and top-view snapshots from one of the 48 human-in-the-loop experiments conducted with 12 participants using the proposed teleoperator-aware CBF-based ANMPC framework. In this trial, the human operator steers the Go2 quadrupedal robot from a designated initial position toward target points, located at the far end of the laboratory, while safely navigating around 10 cylindrical obstacles. The videos are available online [24].

solving highly dynamic, interconnected control problems in real time. For instance, if a human commands a quadruped to step laterally but its legs are not in a feasible stance, executing the command without accounting for the robot's dynamics could lead to instability or even falling.

Most relevant to our shared autonomy approach are related methods that combine intent blending with safety guarantees. [32] introduced a stochastic optimal control framework that couples a noisily rational Boltzmann model of human behavior [33] with shielding-aware robust planning to ensure safe and efficient human–robot interaction under uncertainty. This approach approximates the stochastic optimal control problem using a scenario-tree-based stochastic model predictive control (SMPC) formulation. However, this framework and related methods were primarily developed for autonomous driving contexts and robotic manipulation, and do not address the unique challenges of safe legged locomotion, such as high dimensionality and underactuation. [34] developed an MPC framework that incorporates human input commands to control the front legs of a quadruped rescue robot while autonomously generating back-leg and center of mass (CoM) motions to ensure static stability. However, this approach does not consider teleoperator-aware, safety-critical NMPC for obstacle-avoidance. In addition, [35] proposed a whole-body shared-control framework with bilateral force feedback for obstacle avoidance of a wheeled humanoid robot, but this method does not employ a safety-critical NMPC formulation that explicitly accounts for human intention.

B. Contributions

The *overarching goal* of this paper is to develop a computationally efficient, teleoperator-aware, safety-critical, and adaptive nonlinear model predictive control (ANMPC) framework for shared autonomy of quadrupedal robots performing obstacle-avoidance tasks. The main *contributions* are as follows.

1. *Teleoperator-aware shared autonomy*: The framework employs a fixed arbitration weight between human and robot actions, but enhances this scheme by explicitly modeling human inputs with a noisily rational Boltzmann model. Real-time trajectory planning is then formulated as a CBF-based NMPC for the human–robot system.

2. *Online adaptation*: The human value function is parameterized as a convex function, combining quadratic goal-reaching terms with logarithmic barrier functions for safety. The parameters of this value function are adapted in real time using a projected gradient descent (PGD) law based

on observed joystick commands, enabling the robot to adapt online while maintaining forward invariance of the safety set.

3. *Efficient incorporation of barrier constraints*: Since the inclusion of logarithmic barriers makes prediction of human actions within the NMPC nontrivial, we introduce a computationally efficient method that allows human-aware safety constraints to be incorporated into the NMPC.

4. *Hierarchical control architecture*: The overall control architecture is hierarchical. At the high level, the proposed CBF-based ANMPC generates blended human–robot velocity references at 10 Hz. At the mid level, a dynamics-aware NMPC enforces SRB dynamics to track these references at 60 Hz. At the low level, a nonlinear whole-body controller (WBC) imposes the full-order dynamics via quadratic programming to track the mid-level trajectories at 500 Hz.

5. *Validation on hardware*: The proposed framework is validated through extensive hardware experiments and user studies on the Unitree Go2 quadrupedal robot navigating uncertain environments (see Fig. 1). The results demonstrate real-time obstacle avoidance, online adaptation of human intent parameters, and safe teleoperator–robot collaboration.

II. PROBLEM FORMULATION

A. Robotic Agent and Environment

We consider a general class of nonlinear, input-affine, discrete-time dynamical systems to describe the evolution of the robotic agent:

$$\Sigma: \begin{cases} x(t+1) = f(x(t), u(t)) = a(x(t)) + B(x(t)) u(t) \\ y(t) = C x(t), \end{cases} \quad (1)$$

where $x \in \mathcal{X} \subset \mathbb{R}^{n_x}$ and $u \in \mathcal{U} \subset \mathbb{R}^{n_u}$ denote the state vector and control input, respectively, for some positive integers n_x and n_u . The discrete time index is given by $t \in \mathbb{Z}_{\geq 0} := \{0, 1, \dots\}$. The nonlinear state transition map $f: \mathcal{X} \times \mathcal{U} \rightarrow \mathcal{X}$ is input-affine, i.e., $f(x, u) = a(x) + B(x) u$, with $a(x) \in \mathbb{R}^{n_x}$ and $B(x) \in \mathbb{R}^{n_x \times n_u}$. The output $y \in \mathbb{R}^{n_y}$ encodes the robot's position in the xy -plane and its orientation (yaw angle), with $n_y = 3$, and is obtained through the output mapping $C \in \mathbb{R}^{n_y \times n_x}$.

We focus on shared autonomy in obstacle-avoidance tasks, where the control input to the robotic agent is determined collaboratively by the human and the trajectory planning algorithm. To capture this interaction, the control input is modeled as a weighted combination of the human input $u^H(t)$ and the robot input $u^R(t)$ (i.e., linear policy blending). Here, $u^H(t)$ corresponds to joystick commands provided by the human operator, while $u^R(t)$ denotes the output of

the proposed human-aware, CBF-based, ANMPC algorithm. Specifically, the control input in (1) is given by

$$u(t) = \lambda u^R(t) + (1 - \lambda) u^H(t), \quad (2)$$

where $\lambda \in [0, 1]$ is a weighting factor. The two extreme cases correspond to fully autonomous control when $\lambda = 1$, and fully human control when $\lambda = 0$.

Example 1 (Kinematic Model): As an illustrative case, we consider the kinematic car model:

$$\begin{bmatrix} \dot{p}_x \\ \dot{p}_y \\ \dot{\alpha} \end{bmatrix} = \begin{bmatrix} v \cos(\alpha) \\ v \sin(\alpha) \\ \omega \end{bmatrix}, \quad (3)$$

where $x := \text{col}(p_x, p_y, \alpha) \in \mathbb{R}^3$ denotes the state vector, with p_x and p_y representing the Cartesian coordinates of the robot in the xy -plane and α the yaw angle. Here, “col” denotes the column operator. The control input is given by $u := \text{col}(v, \omega) \in \mathbb{R}^2$, where v and ω denote the linear and angular velocities, respectively. The continuous-time kinematic car model in (3) can be discretized using the Euler method and expressed in the input-affine form of (1).

The target position of the robotic agent is assumed to be known to both the agent and the human operator, and is represented by the vector $g \in \mathbb{R}^3$. This vector encodes the desired Cartesian coordinates of the target in the xy -plane together with the desired orientation (yaw angle). Static obstacles in the xy -plane are represented by their center points $o_\ell \in \mathbb{R}^2$ for $\ell \in \mathcal{O} := \{1, \dots, n_{\mathcal{O}}\}$, where $n_{\mathcal{O}}$ denotes the total number of obstacles. We further assume that the positions of the obstacles are known to both the human operator and the robotic agent.

B. Human Action Model

We aim to design a CBF-based ANMPC algorithm that predicts the human teleoperator’s actions using a parameterized model, while learning and updating the parameters in real time to ensure effective and safe planning for the robotic agent in obstacle-rich environments. To this end, we adopt the noisy rational Boltzmann model, widely used in cognitive science [33]. In this framework, the human selects an action u^H according to a reward-based decision rule:

$$P(u^H | x, \theta) = \frac{e^{-\beta Q(x, u^H, \theta)}}{\int e^{-\beta Q(x, \tilde{u}^H, \theta)} d\tilde{u}^H} = \frac{e^{-\beta Q(x, u^H, \theta)}}{Z(x, \theta)}, \quad (4)$$

where $Q(x, u^H, \theta)$ denotes the human’s state-action value function (equivalently, the negative reward), parameterized by a set of *unknown* and time-varying parameters $\theta \in \mathbb{R}^{n_{\theta}}$, $\beta > 0$ is the rationality coefficient, and $Z(x, \theta) := \int e^{-\beta Q(x, \tilde{u}^H, \theta)} d\tilde{u}^H$. Under this model, the teleoperator selects actions that are exponentially more likely to yield higher rewards (i.e., lower values of Q), that is,

$$u^{H*}(x, \theta) := \arg \max_{u^H} P(u^H | x, \theta) = \arg \min_{u^H} Q(x, u^H, \theta).$$

1) Parametrization of the Human’s Value Function:

We assume that the human’s state-action value function is convex and composed of quadratic terms that minimize the distance between the robot’s output and the target while reducing human effort, and logarithmic barrier functions that penalize collisions with obstacles. More specifically, we

consider the following parameterized human’s value function

$$Q(x, u^H, \theta) := \|C f(x, u^H) - g\|_{M(\theta_1)}^2 + \|u^H\|_{M(\theta_2)}^2 - \theta_3 \sum_{\ell=1}^{n_{\mathcal{O}}} \ln \frac{\|C_{xy} f(x, u^H) - o_\ell\|^2}{d_{\text{th}}^2}, \quad (5)$$

where $C f(x, u^H) \in \mathbb{R}^3$ denotes the predicted position and orientation of the robot at the next time step under the human input, $C_{xy} f(x, u^H) \in \mathbb{R}^2$ represents the corresponding predicted position in the xy -plane (excluding orientation), and d_{th} is a safety distance threshold. In our formulation, the parameter vector is decomposed as $\theta = \text{col}(\theta_1, \theta_2, \theta_3)$, where θ_1 and θ_2 are vectors and θ_3 is a scalar. For each $i \in \{1, 2\}$, we define $M(\theta_i) := \text{diag}(\theta_i)$ as a diagonal matrix with the entries of θ_i on the diagonal. Finally, for any vector z , we use the notations $\|z\|_M^2 := z^\top M z$ and $\|z\|^2 := z^\top z$.

The parameters must be chosen such that $M(\theta_1) > 0$, $M(\theta_2) > 0$, and $\theta_3 > 0$. Under these conditions, the first quadratic term in (5) encourages the robot to approach the target point, the second term penalizes the magnitude of the human action, and the final logarithmic term promotes maintaining a safe distance from obstacles.

2) Parameterized Human Action and Computational Challenge: From the parameterized and convex Q -function in (5), the operator’s optimal action must satisfy the stationarity condition $\nabla_{u^H} Q(x, u^H, \theta) = 0$, which yields the following algebraic equation:

$$\begin{aligned} \varphi(x, u^H, \theta) &:= B^\top C^\top M(\theta_1) (C(a + B u^H) - g) \\ &\quad + M(\theta_2) u^H \\ &\quad - \theta_3 \sum_{\ell=1}^{n_{\mathcal{O}}} \frac{B^\top C_{xy}^\top (C_{xy}(a + B u^H) - o_\ell)}{\|C_{xy}(a + B u^H) - o_\ell\|^2} \\ &= 0. \end{aligned} \quad (6)$$

Thus, for each (x, θ) , we estimate the operator’s input u^{H*} by solving $\varphi(x, u^H, \theta) = 0$. In doing so, we adopt a deterministic NMPC formulation rather than a computationally expensive SMPC, ignoring additional uncertainty in the estimation. Instead, our framework accounts for uncertainty in the parameters of the Q -function, which are updated online. Since the algebraic equation (6) is nonlinear in u^H , no closed-form solution generally exists for u^{H*} , posing a major challenge for designing a human-aware, safety-critical controller. In Section III, we demonstrate how the proposed ANMPC scheme efficiently overcomes this difficulty.

C. Collision Safety and Problem Statement

We define the safe set as the super-level set of the Euclidean distance, ensuring a minimum separation between the agent and all obstacles:

$$\mathcal{S} := \{x \in \mathcal{X} \mid \|C_{xy} x - o_\ell\| \geq d_{\text{th}}, \forall \ell \in \mathcal{O}\}, \quad (7)$$

where $C_{xy} x$ denotes the Cartesian coordinates of the robot in the xy -plane, as introduced earlier. Ensuring system safety in the presence of a human in the loop can be formulated as maintaining the forward invariance of \mathcal{S} [21]. However, designing a safety-critical NMPC law to guarantee this

invariance is challenging because: 1) the parameters of the human's value function θ are generally unknown and time-varying, and 2) the human action must satisfy the algebraic constraint $\varphi(x, u^H, \theta) = 0$, as given in (6), for which no closed-form expression of u^H is available. To overcome these challenges, the algorithm proposed in Section III introduces a computationally efficient ANMPC framework that explicitly accounts for both sources of uncertainty.

The safe set can equivalently be reformulated as

$$\mathcal{S} := \{x \in \mathcal{X} \mid h(x) \geq 0\}, \quad (8)$$

where the continuous function h is defined as

$$h(x) := \text{col}\{h_\ell(x) \mid \ell \in \mathcal{O}\} \in \mathbb{R}^{n_\varphi}, \quad (9)$$

with individual components given by $h_\ell(x) := \|C_{xy} x - o_\ell\| - d_{\text{th}}$. Before establishing the proposed human-aware and safety-critical ANMPC algorithm, we introduce the notion of discrete-time CBFs for the human–robot system.

Definition 1 (Discrete-Time CBF [36]): The function h is said to be a CBF for (1) if there exists a class \mathcal{K} function γ , satisfying $\gamma(s) < s$ for all $s > 0$, such that

$$\Delta h(x(t), u(t)) \geq -\gamma(h(x(t))), \quad \forall x(t) \in \mathcal{X}, \quad (10)$$

where $\Delta h(x(t), u(t)) := h(x(t+1)) - h(x(t)) := h(f(x(t), u(t))) - h(x(t))$.

Lemma 1 (CBF Condition [36]): If h is a discrete-time CBF on \mathcal{X} for (1), then any discrete-time control input $u(t)$ that satisfies (10) renders the set \mathcal{S} forward invariant.

Here, we assume that h has relative degree $r = 1$. Under this assumption, the CBF condition in (10), together with the weighted sum of the human and robot actions in (2), can be expressed as the following inequality constraint

$$\psi(x(t), \lambda u^R(t) + (1 - \lambda) u^H(t)) \geq 0, \quad (11)$$

which must hold for all $t \in \mathbb{Z}_{\geq 0}$.

Problem 1 (Problem Statement): We aim to design a computationally efficient, human-aware, safety-critical, and adaptive NMPC algorithm that computes the optimal robot action $u^R(t) \in \mathcal{U}^R \in \mathbb{R}^{n_u}$ to steer the robotic agent from an initial condition to the target point g , while (i) predicting the human action through the algebraic constraint (6), (ii) ensuring the forward invariance of the safety set \mathcal{S} , and (iii) learning in real time the unknown parameters θ of the human state-action value function.

III. HUMAN-AWARE, SAFETY-CRITICAL ANMPC

This section presents the high-level human-aware, safety-critical ANMPC algorithm, which leverages CBFs for real-time trajectory planning of quadrupedal robots in obstacle-rich environments, as in Problem 1. Let $\hat{\theta}(t) \in \mathbb{R}^{n_\theta}$ denote the estimate of the *unknown*, time-varying parameters $\theta(t)$. The proposed ANMPC algorithm consists of two loops. At each time step t , the *inner loop* is formulated as a human-aware, CBF-based NMPC that optimizes the robot's action subject to the current parameter estimate $\hat{\theta}(t)$. The *outer loop* serves as the learning layer, updating the parameter estimate for the next time step using a PGD method.

A. Inner Loop: CBF-based NMPC

Within the inner loop, our goal is to design a computationally efficient CBF-based NMPC algorithm that incorporates human actions via the algebraic condition (6), given the parameter estimate $\hat{\theta}(t)$ at time t . As noted earlier, no general closed-form solution exists for the optimal human action $u^H(x, \theta)$. While one could attempt to approximate these actions numerically—for example, by gridding the state and parameter spaces and applying machine learning techniques—substituting such approximations into the collaborative dynamics

$$x(t+1) = f(x(t), \lambda, u^R(t) + (1 - \lambda), u^H(x, \hat{\theta}(t))), \quad (12)$$

would introduce additional nonlinearities, thereby increasing the complexity of the NMPC formulation.

As an alternative, we adopt a computationally efficient strategy by incorporating the state equation (1), subject to the condition (2), together with the algebraic constraint (6). In this formulation, the decision variables of the CBF-based NMPC problem consist of the predicted trajectories of the states, the robot control inputs, and the human inputs over the horizon, denoted by $x(\cdot)$, $u^R(\cdot)$, and $u^H(\cdot)$, respectively. This formulation allows the NMPC to solve for the human action implicitly by enforcing the algebraic condition (6) as an equality constraint. Importantly, the output of the NMPC algorithm is the first robot action, while the human action trajectory is discarded—used only to ensure satisfaction of the algebraic constraint and to support parameter estimation. More specifically, we propose the following CBF-based NMPC, given the parameter estimate $\hat{\theta}(t)$ at time t :

$$\begin{aligned} \min_{(x(\cdot), u^R(\cdot), u^H(\cdot), \delta(\cdot))} & \mathcal{L}_{\text{terminal}}^R(x_{t+N|t}) + \sum_{k=0}^{N-1} \mathcal{L}_{\text{stage}}^R(x_{t+k|t}, u_{t+k|t}^R) \\ & + \sum_{k=0}^{N-1} \mathcal{L}_{\text{stage}}^H(u_{t+k|t}^H) + \sum_{k=0}^{N-1} w \delta_{t+k|t}^2 \\ \text{s.t. } & x_{t+k+1|t} = f(x_{t+k|t}, \lambda u_{t+k|t}^R + (1 - \lambda) u_{t+k|t}^H) \\ & \varphi(x_{t+k|t}, u_{t+k|t}^H, \hat{\theta}(t)) = 0 \quad (\text{Human Action}) \\ & \psi(x_{t+k|t}, \lambda u_{t+k|t}^R + (1 - \lambda) u_{t+k|t}^H) \geq \delta_{t+k|t} \mathbf{1} \quad (\text{CBF}) \\ & u_{t+k|t}^R \in \mathcal{U}^R \quad (\text{Feasibility}) \\ & k = 0, 1, \dots, N-1, \end{aligned} \quad (13)$$

where N is the prediction horizon, and $x_{t+k|t}$, $u_{t+k|t}^R$, $u_{t+k|t}^H$, $\delta_{t+k|t}$ denote the predicted states, robot inputs, human inputs, and CBF slack variables at time $t+k$, computed at time t using the prediction model and the algebraic constraint, with $x_{t|t} = x(t)$. The cost function consists of the terminal and stage costs, defined as $\mathcal{L}_{\text{terminal}}^R(x_{t+N|t}) := \|x_{t+N|t} - x_{t+N|t}^{\text{ref}}\|_{P^R}^2$, $\mathcal{L}_{\text{stage}}^R(x_{t+k|t}, u_{t+k|t}^R) := \|x_{t+k|t} - x_{t+k|t}^{\text{ref}}\|_{Q^R}^2 + \|u_{t+k|t}^R\|_{R^R}^2$, $\mathcal{L}_{\text{stage}}^H(u_{t+k|t}^H) := \|u_{t+k|t}^H\|_{R^H}^2$, where $x^{\text{ref}}(\cdot)$ denotes the reference state trajectory for steering the robot to the goal, and P^R , Q^R , R^R , and R^H are symmetric positive-definite matrices. The weighting factor $w > 0$ penalizes slack variables, and $\mathbf{1} := \text{col}(1, \dots, 1)$ is an all-ones vector. The equality constraints of the NMPC originate from the collaborative system dynamics (1) and the gradient-based

law for the human action in (6). The inequality constraints stem from the CBF condition (10) for obstacle avoidance, augmented with a slack variable to ensure feasibility of the NMPC, as well as from the input admissibility condition.

The CBF-based NMPC is solved in a receding-horizon fashion at 10 Hz for a given $\hat{\theta}(t)$. The first optimal robot action, defined as $\pi^R(x, \hat{\theta}(t)) := u_{t|t}^R$, is applied to the robotic system, while the estimated human action $u_{t|t}^H$ is passed to the adaptive law in Section III-B to update the parameter estimate $\hat{\theta}$ for the next time step.

B. Outer Loop: PGD-based Adaptive Law

Within the outer loop, we aim to design a PGD-based adaptive law that updates the estimated parameters of the human's value function using the observed human action. Let $u^H(t)$ denote the actual human action executed by the operator, which can be measured from the joystick. The estimation is updated at each time step based on the most recent human measurement and its deviation from the estimated human action $u_{t|t}^H$. More specifically, we consider the following cost function:

$$J(\hat{\theta}) := \frac{1}{2} \left(u_{t|t}^H - u^H(t) \right)^\top \Gamma \left(u_{t|t}^H - u^H(t) \right), \quad (14)$$

where $u_{t|t}^H - u^H(t)$ represents the deviation between the estimated and observed human actions, and $\Gamma = \Gamma^\top \succ 0$ is a positive definite weighting matrix. Importantly, the cost function $J(\cdot)$ depends on the current estimate $\hat{\theta}(t)$ in a nonlinear manner, since $u_{t|t}^H$ is implicitly determined by $\hat{\theta}(t)$ through the parameterized constraint $\varphi(\cdot, \cdot, \hat{\theta}(t)) = 0$ in the NMPC formulation (13).

To establish the PGD algorithm, we differentiate the cost function with respect to $\hat{\theta}$, yielding

$$\frac{\partial J}{\partial \hat{\theta}}(\hat{\theta}) = \left(u_{t|t}^H - u^H(t) \right)^\top \Gamma \frac{\partial u_{t|t}^H}{\partial \hat{\theta}}, \quad (15)$$

since $u^H(t)$ does not depend on the estimated parameters. Next, we evaluate $\frac{\partial u_{t|t}^H}{\partial \hat{\theta}}$. As the NMPC enforces the algebraic constraint over the prediction horizon, and in particular at time t , we have

$$\varphi(x(t), u_{t|t}^H, \hat{\theta}(t)) = 0, \quad \forall \hat{\theta}(t) \in \Theta, \quad (16)$$

where $\Theta \subset \mathbb{R}^{n_\theta}$ denotes the set of feasible parameters (e.g., nonnegative values). Differentiating both sides of this algebraic constraint with respect to $\hat{\theta}$ gives

$$\frac{\partial \varphi}{\partial u^H} \frac{\partial u_{t|t}^H}{\partial \hat{\theta}} + \frac{\partial \varphi}{\partial \hat{\theta}} = 0. \quad (17)$$

Assuming that $\frac{\partial \varphi}{\partial u^H} \in \mathbb{R}^{n_u \times n_u}$ is invertible, one can explicitly solve for $\frac{\partial u_{t|t}^H}{\partial \hat{\theta}}$ from (17) and substitute it into (15), yielding

$$\frac{\partial J}{\partial \hat{\theta}}(\hat{\theta}) = - \left(u_{t|t}^H - u^H(t) \right)^\top \Gamma \left(\frac{\partial \varphi}{\partial u^H} \right)^{-1} \frac{\partial \varphi}{\partial \hat{\theta}}. \quad (18)$$

Our numerical and experimental results in Section V indicate that this assumption is not restrictive; indeed, the square matrix $\frac{\partial \varphi}{\partial u^H}$ is consistently invertible in practice.

The PGD-based update law is formulated in two steps:

$$\begin{aligned} \eta(t+1) &= \hat{\theta}(t) - \mu(t) \nabla_{\hat{\theta}} J(\hat{\theta}(t)) \\ &= \hat{\theta}(t) + \mu(t) \frac{\partial \varphi}{\partial \hat{\theta}} \left(\frac{\partial \varphi}{\partial u^H} \right)^{-1} \Gamma \left(u_{t|t}^H - u^H(t) \right) \\ \hat{\theta}(t+1) &= \Pi_\Theta(\eta(t+1)) = \arg \min_{z \in \Theta} \|z - \eta(t+1)\|^2, \end{aligned} \quad (19)$$

where $\mu(t)$ is the step size, and $\Pi_\Theta(\cdot)$ denotes the projection operator onto Θ , defined as the closest point in Θ to $\eta(t+1)$ under the Euclidean norm. The updated parameter $\hat{\theta}(t+1)$ is then used in the CBF-based NMPC executed at time $t+1$.

IV. MIDDLE AND LOWER LAYERS OF THE ALGORITHM

This section provides a concise overview of the mid- and low-level layers of the layered control scheme, adapted from [13], [14] with modifications.

Mid-Level NMPC: The control framework employs the proposed human-aware, CBF-based ANMPC algorithm, subject to the kinematic model of the quadrupedal robot provided in Example 1, at the high level of the control hierarchy and running at 10 Hz. This layer generates the reference linear and angular velocities of the robot collaboratively from the actual human action and the ANMPC output, namely,

$$u(t) = \lambda \pi^R(x(t), \hat{\theta}(t)) + (1 - \lambda) u^H(t), \quad (20)$$

where, as discussed earlier, $\pi^R(x(t), \hat{\theta}(t))$ and $u^H(t)$ denote the first optimal action computed by the CBF-based ANMPC and the human action, respectively.

At the mid level of the control scheme, we employ an alternative, dynamics-aware NMPC algorithm running at 60 Hz, which enforces the reduced-order single rigid body (SRB) dynamics of the quadrupedal robot to track the reference trajectories prescribed by the high-level CBF-based ANMPC. More specifically, the mid-level NMPC incorporates the 6-DoF SRB dynamics of the robot, consisting of the translational and rotational motion of the torso subject to ground reaction forces (GRFs) [14]. This layer optimally computes the GRFs to ensure dynamic stability, satisfy friction cone constraints, and track the reference velocity trajectories.

Low-Level Whole-Body Controller: At the low level, we employ a nonlinear WBC that enforces the full-order dynamics of the quadrupedal robot to track the prescribed SRB states and GRFs. The WBC is adopted from [11], [37] and is implemented as a real-time QP running at 500 Hz.

V. EXPERIMENTS

A. Setup and Controller Synthesis

In this paper, we employ the Unitree Go2 quadrupedal robot as the hardware platform for both numerical and experimental validation of the proposed teleoperator-aware CBF-based ANMPC framework. The Go2 is a lightweight, 15.0 kg quadruped with a standing height of 0.28 m and 18 DoFs, including 12 actuated joints—three per leg (hip pitch, hip roll, and knee pitch). For perception, it is equipped with a Unitree L1 4D LiDAR offering $360^\circ \times 90^\circ$ hemispherical coverage, from which a deskewed point cloud is used for obstacle detection. Human teleoperation commands are provided via a Sony DualShock 4 controller, which specifies linear and angular velocities of the robot's torso. The proposed CBF-based ANMPC algorithm is executed offboard

in a multithreaded configuration on a desktop workstation with a 12th Gen Intel® Core™ i9-12900F CPU and 64 GB of RAM, with communication handled over a LAN. For numerical simulations, the RaiSim physics engine [38] is used to evaluate the performance of the control framework.

CBF-based ANMPC Hyperparameters: We set the sampling time to $T_s = 0.1$ s for discretizing the kinematic model in (3), the prediction horizon to $N = 100$, and the teleoperation blend factor to $\lambda = 0.35$ in (2). The gain matrices of the CBF-based NMPC for the kinematic model in Example 1 are specified as $Q^R = \text{diag}\{4, 4, 4\}$, $P^R = \text{diag}\{40, 40, 40\}$, $R^R = \text{diag}\{0.4, 0.2\}$, $Q^H = \text{diag}\{0.02, 0.02\}$, and $w = 10^3$. The safety parameters, including the CBF gain γ and the keep-out radius d_{th} in (7) and (10), are set to $\gamma = 0.1$ and $d_{\text{th}} = 0.5$ m, respectively. For the experimental validation, we parameterize the Q -function in (5) using four parameters. The first quadratic term employs $\theta_1 := \text{col}(\theta_1^x, \theta_1^y, \theta_1^\alpha)$, where $\theta_1^x = \theta_1^y$ correspond to approaching the target in the xy -directions, and θ_1^α corresponds to tracking the target in the yaw direction. A scalar parameter θ_2 captures the human effort cost in both linear and angular velocity commands, while θ_3 parameterizes the logarithmic barrier function for obstacle avoidance. The initial estimates of the human parameters in the PGD-based adaptation law (19) are chosen as $\hat{\theta}_1(0) = \text{col}(\hat{\theta}_1^x(0), \hat{\theta}_1^y(0), \hat{\theta}_1^\alpha(0)) = \text{col}(0.4, 0.4, 5)$, $\hat{\theta}_2(0) = 2$, and $\hat{\theta}_3(0) = 2$. The adaptation parameters are set to $\Gamma = \text{diag}\{0.01, 0.01, 0.01, 0.01, 0.01\}$ and $\mu = 1$. The linear policy blending in (20) is saturated to linear velocities within $[-0.4, 0.4]$ m/s and angular velocities within $[-0.8, 0.8]$ rad/s. The hyperparameters of the mid-level NMPC and the low-level nonlinear WBC are selected based on [14].

Real-Time Computation: The nonlinear program (NLP) in (13) involves 803 decision variables, namely $x(\cdot)$, $u^R(\cdot)$, $u^H(\cdot)$, and $\delta(\cdot)$, together with the initial state of the model, which is constrained to match the measured state feedback at time t . The NLP is implemented in the CasADi framework [39] and solved using the IPOPT solver [40]. Each NMPC iteration is restricted to 10 solver iterations, with the previous solution used as a warm-start initial guess. Importantly, the NLP is solved online without approximations to the nonlinear dynamics, the algebraic constraints induced by the human action, or the CBF constraints. The average solve time of the NLP is 27 ms, and no infeasibility was encountered during the experiments. The mid-level NMPC is likewise implemented in CasADi and solved at 60 Hz, following [14].

B. Human-in-the-Loop Hardware Experiments

Experimental Setup: Human-in-the-loop experiments were conducted in an 8.1×5.4 m² laboratory space with 10 cylindrical obstacles (radius 0.125 m) and two target goals, denoted g_A and g_B (see Fig. 1). Each target specified the desired xy coordinates and yaw angle of the robot and was marked on the floor with an arrow to guide participants. Twelve subjects each completed four trials. In these trials, participants were tasked with steering the robot from a designated initial condition to the target while avoiding obstacles. Specifically, two trials involved fully human (i.e., baseline)

TABLE I
THE QUESTIONS ASKED IN OUR DEMO SURVEY.

Question	
Q1: I could command the robot to do what I intended with ease.	
Q2: I could feel the assistive movements from the robot.	
Q3: Autonomy assisted me in completing the task.	

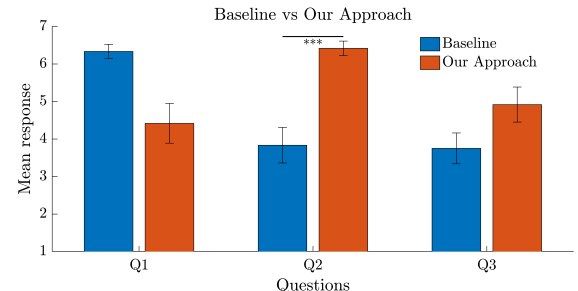


Fig. 2. Results of the post-demo survey with questions in Table I comparing the proposed shared control with the baseline control for the target g_A .

control toward g_A and g_B (i.e., $\lambda = 0$), while the remaining two trials employed shared autonomy, in which the proposed high-level CBF-based ANMPC assisted navigation toward g_A and g_B (i.e., $\lambda = 0.35$). During all trials, the operator stood at the side of the lab with an unobstructed view of the space. To mitigate ordering effects, trial sequences were randomized uniformly. In total, 48 experiments were conducted: 24 under baseline control and 24 under shared autonomy. Participants were not informed which control mode was active in each trial, ensuring unbiased interaction.

Quantitative Analysis: Across all 48 trials, the human subjects successfully and safely navigated the quadrupedal robot toward both designated goals. After completing each pair of experiments for a given target—one under fully human control and the other under shared autonomy—the participants completed a survey questionnaire to evaluate the performance of each control method, as shown in Table I. Responses were recorded on a 7-point Likert scale, where subjects indicated their level of agreement: Strongly Disagree (1), Disagree (2), Slightly Disagree (3), Neutral (4), Slightly Agree (5), Agree (6), or Strongly Agree (7). Figure 2 illustrates the results of the post-demo survey. The plot indicates that users generally reported feeling more comfortable and at ease when using the baseline controller compared to the shared autonomy mode. This outcome is largely attributed to the fact that participants were not informed about which controller was active during each trial; as a result, in some cases, their actions conflicted with the assistance provided by the shared autonomy algorithm, as they attempted to override or correct it to follow their intended commands. Nevertheless, participants reported that the assistive behaviors introduced by shared autonomy were perceptible during the task (paired t-test, $p < 0.001$). They also found shared autonomy beneficial, helping them complete the task.

To quantitatively compare system responses under the proposed shared autonomy and baseline control, Fig. 3 shows the human-commanded velocity inputs $u^H = \text{col}(v^H, \omega^H)$ recorded from a representative subject while steering the robot toward target g_A . In the shared autonomy case, the figure also overlays the predicted human inputs generated

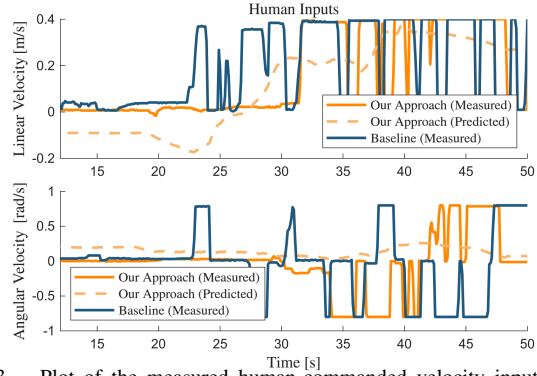


Fig. 3. Plot of the measured human-commanded velocity inputs under the proposed shared autonomy framework and the baseline control method, recorded from a representative subject while steering the robot toward target g_A . The figure also illustrates the predicted human inputs generated by the Boltzmann model in the CBF-based ANMPC algorithm.

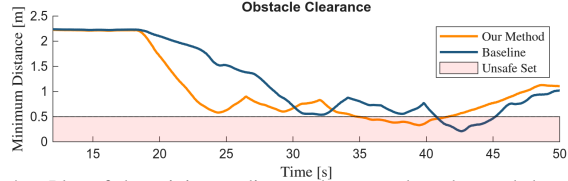


Fig. 4. Plot of the minimum distance between the robot and the nearest obstacle under the proposed teleoperator-aware CBF-based ANMPC (shared autonomy) and the baseline controller (fully human control).

by the ANMPC framework using the Boltzmann model, demonstrating the framework's ability to approximate and adapt to operator behavior in real time—most notably in the linear velocity command. The results further highlight that, with the CBF-based ANMPC, the robot initiates navigation with a trotting gait and requires minimal human intervention until approximately $t = 30$ s. In contrast, under the baseline controller, the human operator must provide continuous input to prevent the robot from trotting in place.

To evaluate safety performance, Fig. 4 plots the minimum distance between the robot and the obstacles. As shown, the proposed CBF-based ANMPC maintains larger safety margins than the baseline controller, thereby enabling more reliable obstacle avoidance. It is worth noting, however, that because slack variables are introduced to relax the CBF constraints and ensure feasibility of the ANMPC optimization, the guaranteed safe distance of $d_{\text{th}} = 0.5$ m is slightly compromised, as reflected in Fig. 4. Finally, the time evolution of the estimated parameters $\hat{\theta}$, updated via the proposed PGD-based adaptation law, is shown in Fig. 5. Parameter updates occur only when the human provides joystick inputs, and the process pauses whenever no command is issued, with λ set to 1. For instance, as observed in Fig. 5, no updates are applied for $t < 30$ s since the human does not issue any significant control commands during that interval.

C. Ablation Study, Discussion, and Future Work

We conducted extensive simulations and human-in-the-loop experiments to analyze the effect of controller hyper-parameters. The arbitration weight λ played a critical role in balancing human influence with autonomy. At $\lambda = 0.5$, human and ANMPC actions often canceled out, reducing operator control, while $\lambda = 0.1$ gave the human excessive authority at the cost of reliable obstacle avoidance. A com-

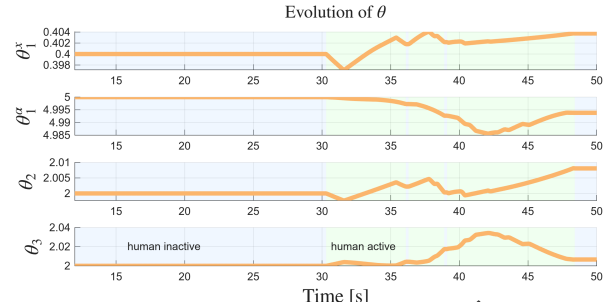


Fig. 5. Time evolution of the estimated parameters $\hat{\theta}$ under the shared autonomy setting, updated online via the PGD-based adaptation law.

promise value of $\lambda = 0.35$ provided an effective balance and was used for all user studies. Similarly, CBF slack variables were essential for feasibility when $\lambda < 0.5$. The slack penalty w determined how much violation was tolerated: high values (10^4) ensured strong safety but resisted the operator, while low values (10) allowed unsafe behavior. We found $w = 10^3$ offered a good balance. The CBF threshold $d_{\text{th}} = 0.5$ m was selected to minimize human opposition in narrow passages, though IMU drift occasionally caused minor collisions when the robot traveled farther than 6 m. The PGD-based update law was tuned via simulation. We chose the above-mentioned Γ matrix to achieve stable convergence for typical users, and initialized θ with steady-state values observed in extended trials. As a result, in human-subject experiments, the estimated parameters changed little, reflecting a near-optimal initialization. These design choices allowed the shared autonomy controller to achieve a 100% success rate in reaching goals across all trials.

Beyond numerical performance, user studies revealed insights into human-robot interaction. Some participants—particularly novices—treated the task like car driving, favoring straight paths and avoiding in-place yaw rotations, which led to suboptimal trajectories that conflicted with the ANMPC predictions. In several cases, users attempted to override the autonomy rather than let it assist, revealing a mismatch between user intuition and the shared autonomy framework. These findings highlight the importance of user training and improved transparency of the autonomy. Overall, the results demonstrate that the proposed controller provides robust safety guarantees and effective shared autonomy, with future work aimed at reducing drift through better state estimation and enhancing user collaboration through training.

VI. CONCLUSIONS

This paper introduced a teleoperator-aware, CBF-based ANMPC framework for shared autonomy of quadrupedal robots performing obstacle-avoidance tasks. The framework employs a fixed arbitration weight to blend human and robot actions, but enhances this strategy by explicitly modeling human inputs with a noisily rational Boltzmann model. The parameters of this model are adapted online using a PGD law informed by observed joystick commands. Safety is guaranteed by embedding CBF constraints into a computationally efficient NMPC despite uncertainty in human behavior. The control architecture is hierarchical: a high-level CBF-based ANMPC (10 Hz) generates blended hu-

man–robot velocity references; a mid-level dynamics-aware NMPC (60 Hz) enforces reduced-order SRB dynamics; and a low-level nonlinear WBC (500 Hz) applies QP to track the mid-level trajectories under full-order dynamics. The proposed framework was validated through extensive hardware experiments, and a user study on the Go2 quadrupedal robot, demonstrating real-time obstacle avoidance, online adaptation of human intent parameters, and safe human–robot collaboration. An ablation study further analyzed the effect of controller hyperparameters on feasibility and success rate.

REFERENCES

- [1] R. Full and D. Koditschek, “Templates and anchors: Neuromechanical hypotheses of legged locomotion on land,” *Journal of Experimental Biology*, vol. 202, no. 23, pp. 3325–3332, 1999.
- [2] S. Kajita and K. Tani, “Study of dynamic biped locomotion on rugged terrain-derivation and application of the linear inverted pendulum mode,” in *IEEE International Conference on Robotics and Automation*, 1991, pp. 1405–1406.
- [3] G. Gibson, O. Dosunmu, Y. Gong, and J. Grizzle, “Terrain-adaptive, ALIP-based bipedal locomotion controller via model predictive control and virtual constraints,” in *IEEE/RSJ International Conference on Intelligent Robots and Systems (IROS)*, 2022, pp. 6724–6731.
- [4] H. Geyer, A. Seyfarth, and R. Blickhan, “Compliant leg behavior explains basic dynamics of walking and running,” *Proceedings. Biological sciences / The Royal Society*, vol. 273, pp. 2861–7, 08 2006.
- [5] Z. Li, J. Zeng, S. Chen, and K. Sreenath, “Autonomous navigation of underactuated bipedal robots in height-constrained environments,” *The International Journal of Robotics Research*, vol. 42, no. 8, pp. 565–585, 2023.
- [6] X. Xiong and A. Ames, “3-D underactuated bipedal walking via H-LIP based gait synthesis and stepping stabilization,” *IEEE Transactions on Robotics*, vol. 38, no. 4, pp. 2405–2425, 2022.
- [7] D. E. Orin, A. Goswami, and S.-H. Lee, “Centroidal dynamics of a humanoid robot,” *Autonomous robots*, vol. 35, no. 2, pp. 161–176, 2013.
- [8] J. Di Carlo, P. M. Wensing, B. Katz, G. Bledt, and S. Kim, “Dynamic locomotion in the MIT Cheetah 3 through convex model-predictive control,” in *IEEE/RSJ International Conference on Intelligent Robots and Systems (IROS)*, Oct 2018, pp. 1–9.
- [9] M. Chignoli and P. M. Wensing, “Variational-based optimal control of underactuated balancing for dynamic quadrupeds,” *IEEE Access*, vol. 8, pp. 49 785–49 797, 2020.
- [10] Y. Ding, A. Pandala, C. Li, Y.-H. Shin, and H.-W. Park, “Representation-free model predictive control for dynamic motions in quadrupeds,” *IEEE Transactions on Robotics*, vol. 37, no. 4, pp. 1154–1171, 2021.
- [11] A. Pandala, R. T. Fawcett, U. Rosolia, A. D. Ames, and K. A. Hamed, “Robust predictive control for quadrupedal locomotion: Learning to close the gap between reduced-and full-order models,” *IEEE Robotics and Automation Letters*, vol. 7, no. 3, pp. 6622–6629, 2022.
- [12] L. Amanzadeh, T. Chunawala, R. T. Fawcett, A. Leonessa, and K. Akbari Hamed, “Predictive control with indirect adaptive laws for payload transportation by quadrupedal robots,” *IEEE Robotics and Automation Letters*, vol. 9, no. 11, pp. 10 359–10 366, 2024.
- [13] B. M. Imran, R. T. Fawcett, J. Kim, A. Leonessa, and K. Akbari Hamed, “A Distributed Layered Planning and Control Algorithm for Teams of Quadrupedal Robots: An Obstacle-Aware Nonlinear MPC Approach,” *Journal of Dynamic Systems, Measurement, and Control*, vol. 147, no. 3, 2025.
- [14] B. M. Imran, J. Kim, T. Chunawala, A. Leonessa, and K. Akbari Hamed, “Safety-critical and distributed nonlinear predictive controllers for teams of quadrupedal robots,” *IEEE Robotics and Automation Letters*, vol. 10, no. 9, pp. 9176–9183, 2025.
- [15] S. Hong, J.-H. Kim, and H.-W. Park, “Real-time constrained nonlinear model predictive control on $SO(3)$ for dynamic legged locomotion,” in *IEEE/RSJ International Conference on Intelligent Robots and Systems (IROS)*, 2020, pp. 3982–3989.
- [16] R. Grandia, A. J. Taylor, A. D. Ames, and M. Hutter, “Multi-layered safety for legged robots via control barrier functions and model predictive control,” in *IEEE International Conference on Robotics and Automation*, 2021, pp. 8352–8358.
- [17] Q. Liao, Z. Li, A. Thirugnanam, J. Zeng, and K. Sreenath, “Walking in narrow spaces: Safety-critical locomotion control for quadrupedal robots with duality-based optimization,” in *IEEE/RSJ International Conference on Intelligent Robots and Systems*, 2023, pp. 2723–2730.
- [18] R. Grandia, F. Jenelten, S. Yang, F. Farshidian, and M. Hutter, “Perceptive locomotion through nonlinear model-predictive control,” *IEEE Transactions on Robotics*, vol. 39, no. 5, pp. 3402–3421, 2023.
- [19] J.-P. Sleiman, F. Farshidian, M. V. Minniti, and M. Hutter, “A unified MPC framework for whole-body dynamic locomotion and manipulation,” *IEEE Robotics and Automation Letters*, vol. 6, no. 3, pp. 4688–4695, 2021.
- [20] A. Meduri, P. Shah, J. Viereck, M. Khadiv, I. Havoutis, and L. Righetti, “BiConMP: A nonlinear model predictive control framework for whole body motion planning,” *IEEE Transactions on Robotics*, vol. 39, no. 2, pp. 905–922, 2023.
- [21] A. D. Ames, X. Xu, J. W. Grizzle, and P. Tabuada, “Control barrier function based quadratic programs for safety critical systems,” *IEEE Transactions on Automatic Control*, vol. 62, no. 8, pp. 3861–3876, Aug 2017.
- [22] L. Wang, A. D. Ames, and M. Egerstedt, “Safety barrier certificates for collisions-free multirobot systems,” *IEEE Transactions on Robotics*, vol. 33, no. 3, pp. 661–674, 2017.
- [23] J. Zeng, B. Zhang, and K. Sreenath, “Safety-critical model predictive control with discrete-time control barrier function,” in *American Control Conference (ACC)*, 2021, pp. 3882–3889.
- [24] Teleoperator-aware and safety-critical adaptive nonlinear MPC for shared autonomy of legged robots. [Online]. Available: <https://youtu.be/gC4sUGGqmzl>.
- [25] A. D. Dragan and S. S. Srinivasa, “A policy-blending formalism for shared control,” *The International Journal of Robotics Research*, vol. 32, no. 7, pp. 790–805, 2013.
- [26] S. Javdani, H. Admoni, S. Pellegrinelli, S. S. Srinivasa, and J. A. Bagnell, “Shared autonomy via hindsight optimization for teleoperation and teaming,” *The International Journal of Robotics Research*, vol. 37, no. 7, pp. 717–742, 2018.
- [27] G. Hoffman, T. Bhattacharjee, and S. Nikolaidis, “Inferring human intent and predicting human action in human–robot collaboration,” *Annual Review of Control, Robotics, and Autonomous Systems*, vol. 7, 2024.
- [28] A. Jonnavaittula, S. A. Mehta, and D. P. Losey, “SARI: Shared autonomy across repeated interaction,” *ACM Transactions on Human-Robot Interaction*, vol. 13, no. 2, pp. 1–36, 2024.
- [29] K. Muelling, A. Venkatraman, J.-S. Valois, J. E. Downey, J. Weiss, S. Javdani, M. Hebert, A. B. Schwartz, J. L. Collinger, and J. A. Bagnell, “Autonomy infused teleoperation with application to brain computer interface controlled manipulation,” *Autonomous Robots*, vol. 41, no. 6, pp. 1401–1422, 2017.
- [30] S. Reddy, A. D. Dragan, and S. Levine, “Shared autonomy via deep reinforcement learning,” *arXiv preprint arXiv:1802.01744*, 2018.
- [31] A. Broad, T. Murphey, and B. Argall, “Learning models for shared control of human-machine systems with unknown dynamics,” in *Proceedings of Robotics: Science and Systems (RSS)*, 2018.
- [32] H. Hu, K. Nakamura, and J. F. Fisac, “SHARP: Shielding-aware robust planning for safe and efficient human–robot interaction,” *IEEE Robotics and Automation Letters*, vol. 7, no. 2, pp. 5591–5598, 2022.
- [33] R. D. Luce, *Individual Choice Behavior: A Theoretical Analysis*. Oxford, U.K.: Wiley, 1959.
- [34] R. Chipalkatty, H. Daepp, M. Egerstedt, and W. Book, “Human-in-the-loop: MPC for shared control of a quadruped rescue robot,” in *IEEE/RSJ International Conference on Intelligent Robots and Systems*, 2011, pp. 4556–4561.
- [35] D. Baek, Y.-C. Chang, and J. Ramos, “A study of shared-control with bilateral feedback for obstacle avoidance in whole-body telelocomotion of a wheeled humanoid,” *IEEE Robotics and Automation Letters*, vol. 8, no. 11, pp. 6979–6986, 2023.
- [36] Y. Xiong, D.-H. Zhai, M. Tavakoli, and Y. Xia, “Discrete-time control barrier function: High-order case and adaptive case,” *IEEE Transactions on Cybernetics*, vol. 53, no. 5, pp. 3231–3239, 2023.
- [37] R. T. Fawcett, A. Pandala, A. D. Ames, and K. Akbari Hamed, “Robust stabilization of periodic gaits for quadrupedal locomotion via QP-based virtual constraint controllers,” *IEEE Control Systems Letters*, pp. 1736–1741, 2021.
- [38] J. Hwangbo, J. Lee, and M. Hutter, “Per-contact iteration method for solving contact dynamics,” *IEEE Robotics and Automation Letters*, vol. 3, no. 2, pp. 895–902, April 2018.

- [39] J. A. E. Andersson, J. Gillis, G. Horn, J. B. Rawlings, and M. Diehl, “CasADi – A software framework for nonlinear optimization and optimal control,” *Mathematical Programming Computation*, vol. 11, no. 1, pp. 1–36, 2019.
- [40] A. Wächter and L. T. Biegler, “On the implementation of an interior-point filter line-search algorithm for large-scale nonlinear programming,” *Mathematical programming*, vol. 106, pp. 25–57, 2006.